Challenges in high NA, polarization, and photoresists

Bruce W. Smith[*a], Julian Cashmore[**b]
[a]Rochester Institute of Technology, Microelectronic Engineering Dept., Rochester, NY
[b]Exitech Limited, Oxford UK

ABSTRACT

Optical lithography is being pushed into a regime of extreme-numerical aperture (extreme-NA). The implications of the nonscalar effects of high-NA lithography (above 0.50) have been discussed now for many years[1]. This paper considers the consequences of imaging at numerical apertures above 0.70 with the oblique imaging angles required for low k_1 lithography. A new scaling factor, k_{NA}, is introduced to capture the impact of low k_1 imaging combined with extreme-NA optics. Extreme-imaging is defined as k_1 and k_{NA} values approach 0.25. Polarization effects combined with resist requirements for extreme-NA are addressed, especially as they relate to 157nm lithography. As these technologies are pursued, careful consideration of optical and resist parameters is needed. Conventional targets for resist index, absorption, diffusion, and reflectivity based on normal incidence imaging may not lead to optimum performance without these considerations. Additionally, methods of local and semi-local mask polarization are discussed using concepts of wire-grid polarizer arrays. Back-side and image-side polarization OPC methods are introduced.

1. INTRODUCTION

Lithographic imaging using projection optics with numerical aperture (NA) values above 0.70 has become a reality for current and future generation devices. What was once considered high-NA (values above 0.60) is now commonplace and the designation needs to be redefined. Historically, the adequacy of scalar diffraction modeling has determined the high-NA regime. Scalar approximations become inaccurate as several optical effects become important. In particular, these are radiometric effects because of optical reduction [2], vectorial effects because of electric field angles [3], and resist effects because of large interference angles [4]. The point at which these effects become significant for optical lithography has been near NA values of 0.60. High-NA corrections, full scalar models, and full vector models have been developed to account for these effects [5]. Though lithography model limits are important, lithographic imaging should be used to define imaging limitations. Though a difficult generalization to make, (and ultimately at the heart of this paper), lithographic imaging with NA values above 0.70 will lead to results that cannot be extrapolated from those achieved with lower values. Imaging effects from oblique angles, electric field polarization, optical interference, optical reflection, and aberration can be significant. A separate designation is proposed for numerical aperture values above 0.70. Since we have come to define high-NA is the range above 0.60, we will define the regime above 0.70 as *extreme-NA*.

We need to describe more than the full numerical aperture of an optical system to understand the impact of extreme-NA. To appreciate the imaging consequences of a given lens pupil, we need to consider imaging situations that make use of the most oblique angles of the lens. In lithographic terms, we are concerned with images corresponding to Rayleigh k_1 values near $0.5/(\sigma+1)$. However, simple use of the Rayleigh k_1 factor is not adequate to describe the NA consequences. Consider for example three imaging situations for 193nm lithography:

a) 0.225 μm (1:1) geometry at 0.30 NA, k_1=0.35
b) 0.113 μm (1:1) geometry at 0.60 NA, k_1=0.35
c) 0.075 μm (1:1) geometry at 0.90 NA, k_1=0.35

In each of these cases, a k_1 factor of 0.35 represents high-resolution imaging. (Note that k_1 is defined here as a half-pitch scaling factor). It fails to describe the differences in the level of difficulty imparted by the lens for the largest NA values. Additional insight is allowed through rearrangement of the Rayleigh condition:

[*] bwsemc@rit.edu, Rochester Institute of Technology, Microelectronic Engineering Dept., 82 Lomb Memorial Dr., Rochester, NY 14623
[**] j.cashmore@exitech.co.uk, Exitech Limited, Hanborough Park, Long Hanborough, Oxford OX8 8LH

$$k_{NA} = \frac{k_1}{NA} = \frac{p}{2\lambda} \geq 0.25$$

Substituting into the three imaging systems described above yields:

a) 0.225 μm (1:1) geometry at 0.30 NA, k_1=0.35, k_{NA}=1.17 (low-NA)
b) 0.113 μm (1:1) geometry at 0.60 NA, k_1=0.35, k_{NA}=0.58 (high-NA)
c) 0.075 μm (1:1) geometry at 0.90 NA, k_1=0.35, k_{NA}=0.39 (extreme-NA)

The optical microlithography community therefore has entered extreme-NA generations where:

$$0.25 < k_1 < 0.35 \text{ and}$$
$$0.25 < k_{NA} < 0.45$$

Figure 1 shows data from the ITRS roadmap for lithography from 1997 to 2009. [6] The plot is not displayed conventionally but instead shows the progress of the k_1 and k_{NA} factors through 248nm, 193nm, and 157nm wavelength technology. By using the above definitions for NA generations, it becomes evident that extreme-NA will be needed in 2003 for 248nm lithography, in 2005 for 193nm lithography, and from the very start of 157nm production lithography. It is therefore critical that we begin considering the impact of extreme-NA on lithography. Specific optical and resist implications should therefore be evaluated.

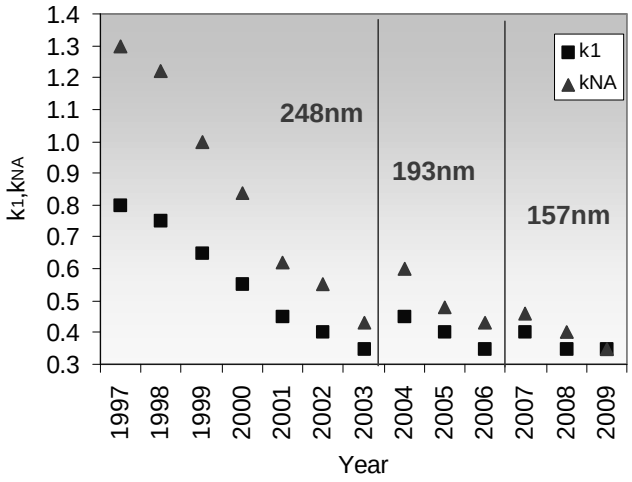

Figure 1. The ITRS roadmap for lithography indicating the progress of k_1 and k_{NA}.

2. IMAGING NEAR k_{NA} OF 0.25

Imaging using low k_1 and low k_{NA} should be evaluated based on the use of the most oblique angles allowed by objective lens and condenser lens pupils. To produce useful lithographic images for low k_1, phase shift masking (PSM), off-axis illumination (OAI), or other high-order capture approaches are utilized. Figure 2 shows an example of the diffraction order collection for a k_1 value near 0.25. The objective lens pupil captures only part of the first diffraction orders spread by a partial coherence factor (σ) of 1.0. Since no other part of these orders is matched with zeroth diffraction order, the best image quality will be achieved by excluding all but these most oblique portions from the illuminator [7]. This is carried out using off-axis illumination (dipole, quadrupole, or annular for example) or similarly using phase shift masking (where zero diffraction order is reduced or eliminated). The concept of extreme-imaging evolves, where low k_1 and low k_{NA} are approached by confining diffraction information to the edge of the projection lens pupil. This information is responsible for the most useful portion of the lithographic image.

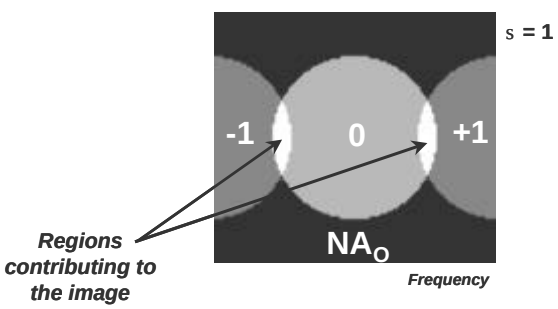

Figure 2. Diffraction order capture for imaging near k_1 and k_{NA} of 0.25. The outer edge of the 1st diffraction orders are collected by the projection lens.

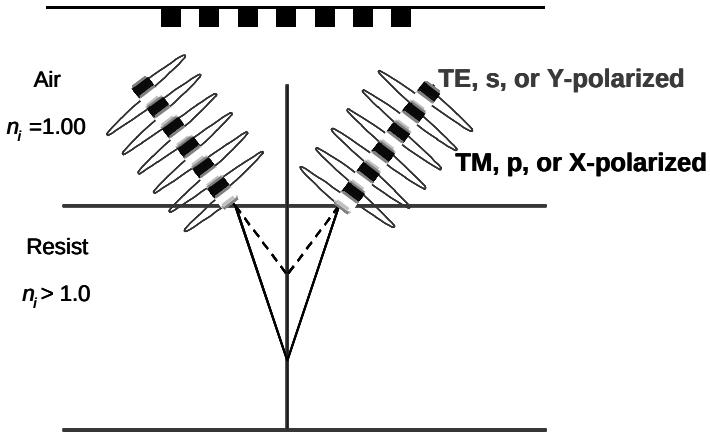

Figure 3. conventions for two states of linear polarization.

2.1 Extreme-imaging and polarization

The propagation angles of the electric field for extreme-NA become significant. At oblique angles, radiation polarized in the plane of incidence exhibits reduced image contrast as interference is reduced. This is referred to as TM, p, or X polarization with respect to vertically oriented geometry. As angles approach *p/4* [or $sin^{-1}(1/\sqrt{2})$], no interference is possible and image contrast in air is reduced to zero. If the image is translated into a media of higher index, the limiting angle is increased by the media index (*n*) as $sin^{-1}(n/\sqrt{2})$. For polarization perpendicular to the plane of incidence, complete interfere exists and no reduction in image contrast will result. Figure 3 shows the two states of linear polarization that contribute to a mask function oriented out of the plane of the page. TM (or X) polarization is in the plane of the page while TE (or Y) polarization is perpendicular. For non-linear polarization, an image is formed as the sum of TE and TM image states.

Extreme-imaging with extreme-NA will result in oblique propagation angles. Figure 4 shows how the power in extreme images is influenced by polarization and NA [8]. These intensity (aerial) images are for $k_1 = 0.25$, which is achieved by oblique illumination at angles that distribute diffraction orders to the edge of the objective lens pupil. This is accomplished for example by using illumination with poles at sigma locations of $1/2pNA$, where *p* is the geometry pitch. Three k_{NA} conditions are shown , 0.5, 0.35, and 0.25 corresponding to NA values of 0.50, 0.707 (or $1/\sqrt{2}$), and 1.0 respectively. Aerial images using TE (or Y) polarization and TM (or X) polarization are shown. There are significant differences in the images in air at a k_{NA} value of 0.5. At a k_{NA} value of 0.35, the X polarization image vanishes as no interference is possible. At a k_{NA} value of 0.25, the contrast of the X polarization is reversed. Once these images are translated into resist (with a refractive index of 1.5 and zero absorbance), X polarization contrast loss is reduced. Image modulation exists at a k_{NA} of 0.35 and image reversal is prevented at a k_{NA} of 0.25. These conditions represent a lower NA condition in the photoresist, resulting from the media index value >1.0.

The significance of these results is the inadequacy of aerial images (in air) for prediction of image performance in resist. An image is formed as the sum of X and Y polarized images. Aerial image evaluation would over-predict degradation from the X polarization in an otherwise unpolarized imaging situation. Furthermore, aerial image evaluation would fail to consider the weighting of the X and Y polarization states that contribute to image formation within a photoresist material. Lithography has traditionally used aerial image metrics such as image contrast or image log-slope [9]. Such aerial image metrics are not useful for extreme NA and polarization. Characterization of alternative image modes needs to be considered.

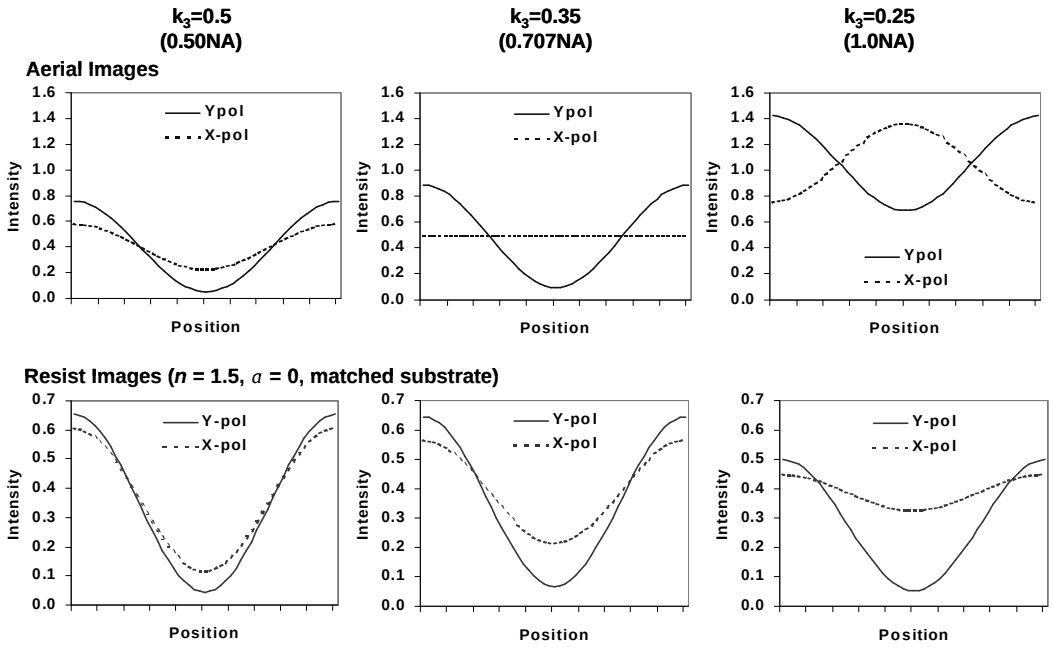

Figure 4. The power (intensity) in extreme images for k_{NA} values from 0.5 to 0.25 for air and resist media.

2.2 Image modes in air and resist

The aerial image log slope is a useful metric for evaluating the quality of an intensity image in air. Translation of an image into a non-absorbing media with an index greater than unity would allow for continued use of this metric to indicate performance. Images within an absorbing photoresist need to be evaluated in terms of the gradients within the resist after absorption and diffusion effects. A resist image, *RI*, can be generalized by considering the influence of the aerial image, *I(n,r,z)*, the absorption of the image through the resist, *exp(-az)*, the diffusion of the image in the resist, $exp(-|Ar/L_d|^2)$, spherical aberration effects induced by the resist as a "plane-parallel plate"[10], $a_s(n,r,z)$, the resist contrast, *g(z)*, and the fractional weighting of polarization components of the image within the resist, f_{TE} *and* f_{TM}. This is shown in Equation 1, where *n* is refractive index, *a* is absorption, *r* is position, *z* is depth, and L_d is diffusion length. Convolution of images with diffusion and aberration functions is represented by the symbol "$*$" [11].

$$RI(r,z) = \left[f_{TE}\left[(I_{TE}(n,r,z)\times e^{-\alpha z}) * e^{-\left|A\frac{r}{L_d}\right|^2} * a_s(n,r,z)\right] + f_{TM}\left[(I(n,r,z)\times e^{-\alpha z}) * e^{-\left|A\frac{r}{L_d}\right|^2} * a_s(n,r,z)\right] \right] \times \gamma(z) \quad (1)$$

This general model gives insight into what needs to be considered as extreme-NA lithography is pursued. Each aspect of the image process can be described individually.

2.2.1 Fractional polarization weighting

Most lithographic systems will use either unpolarized (or circularly polarized) radiation for imaging. For near normal incidence, a resist image can also be considered unpolarized. At non-zero incidence, however, polarization separation of TE and TM components results from reflection at the resist-air interface.[12] As incidence angle is increased to $tan^{-1}(n)$, the electric vector of the reflected radiation has no component in the plane of incidence (an effect first noted by D. Brewster in 1815 and referred to as the Brewster angle). Figure 5 is a plot showing the power into a resist film for

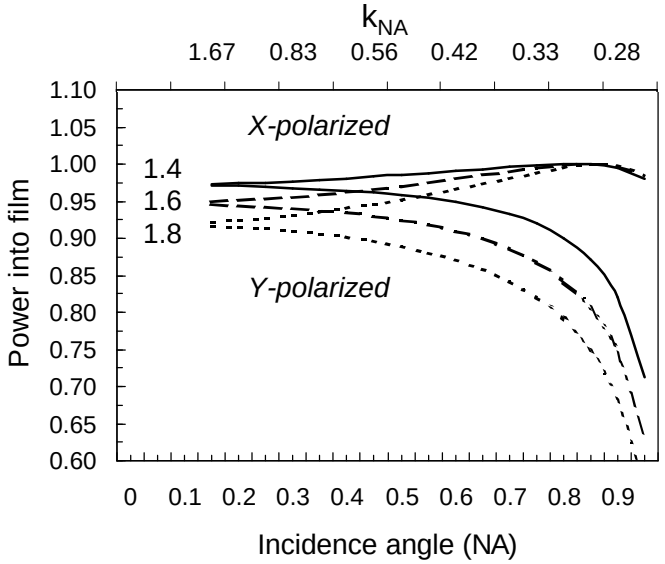

Figure 5. Power transferred (1-R) into resist films with index values from 1.4 to 1.8.

refractive index values between 1.4 and 1.8, which is a range that covers most photoresist material index values for UV/VUV wavelengths. The power is defined as *1-R* (where *R* is reflectivity), which is plotted for numerical aperture values from 0 to 1.0 and k_{NA} values from 0.25 and larger for k_1 values of 0.25. The TM (or X) polarization state (which exists with reduced contrast) is more efficiently coupled into the photoresist film at increasing angles. For extreme-imaging, where oblique imaging angles are used, the TM component is weighed more heavily than the TE (or Y) component, giving rise to degraded image performance. The effect is worsened with higher index resist materials. Table 1 summarizes the fractional weighting of the TM image component for three index values at the corresponding Brewster angle and at 0.95NA.

	Refractive Index		
	1.4	1.6	1.8
Brewster	53%	55%	57%
0.95NA	58%	62%	64%

Table 1. TM image weighting in resist for index values between 1.4 and 1.6 for Brewster angle and 0.95NA.

This represents an undesirable situation as the lower contrast TM image dominates with larger angle and with larger index. There are additional implications with regard to any partial polarization within the imaging system. Though small levels of partial polarization and small across-field variation may be tolerable in terms of aerial image performance, the combination with polarization upon reflection may be detrimental. Reduction of the effect is possible by choosing resist materials with lower refractive index values. This may be difficult as resist platforms are generally chosen based on imaging, transmission, and process performance. Historically, the refractive index values of photoresists has remained near 1.70 for vis/UV/DUV/VUV wavelength technology from 436nm to 157nm (which is merely coincidental since these resists represent a wide array of polymer systems). A more practical solution to the situation is the application of an efficient top anti-reflective coating that is tailored for the large angles encountered in a particular imaging process.

2.2.2 Influence of resist refractive index

As shown in Figure 4, the image produced in a projection system is influence by the index of the imaging media. This represents a lower NA condition for media with index values greater than 1.0 (as governed by Snell's law). Consequently, the influence of polarization is reduced. The impact of imaging is twofold. First, the image contrast loss in TM polarized images is lessened as index is increased. It would be expected, therefore, that any polarization weighting resulting from the imaging system or from reflection would be less significant. Second, as index is increased, the spherical aberration induced by the photoresist increases. This will be address later in more detail but is noted here for description of image performance. Figure 6 shows image gradient plots for TE (or Y) and TM (or X) polarized images in non-absorbing resist films with index values between 1.0 and 1.8.[7] An extreme-imaging case is chosen for a wavelength of 157nm and a lens NA of 0.85, where 60nm 1:1 line features correspond to a k_1 value of 0.32. An illumination condition using an annular source is used with an outer σ value of 0.9 and an inner σ of 0.6. The corresponding k_{NA} is 0.38. For each case, the films are placed over index match substrates. Image depth is also normalized for resist index where a depth value of 0.5 μm represents the best focus position for every condition. Image gradient is defined as *dlnI(x)/dx* at the transition between the line and space region on the mask. The TM polarization images show how increasing the refractive index is beneficial as the consequential reduction in propagation angles improves image quality. Comparison to TE polarization images shows the significance of this improvement, where an index value of 1.8 results in nearly matched behavior between the two polarization states. There is an opposite impact to TE images with increasing index, however. The maximum image gradient can be achieved with the lowest media index value. Increasing the index results in a lowering of the gradient at best focus (0.5 μm depth) but an increase in image gradient throughout the resist depth. This is a direct consequence of spherical aberration and the difference in optical path lengths of zero and first diffraction orders. If the radial locations of each order within the lens pupil were identical, this effect would not exist. This could only be achieved with zero pole width dipole illumination. Since this example uses annular illumination, there is a radial distribution of zero and first order that is unmatched to some extent. The result is a radially dependant phase term, or a spherical aberration effect.

Two generalizations could be made from these results. It appears that reduction in polarization effects is best dealt with by using resist materials with as high an index as possible. On the other hand, if polarized imaging is pursued, and a limited image depth is adequate, lower index materials may be desirable for TE imaging.

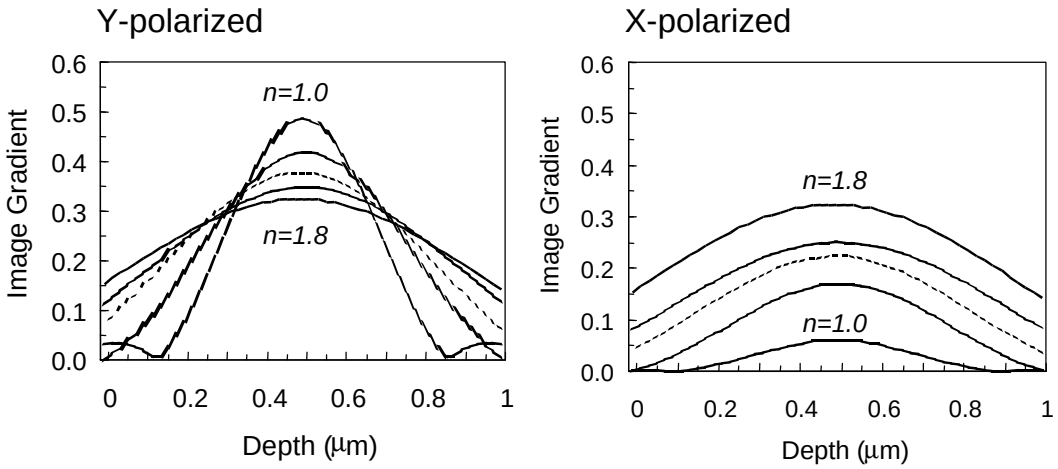

Figure 6. Image gradient plots in resist with refractive index values from 1.0 to 1.8 for Y (TE) polarized and X (TM) images.

2.2.3 Influence of resist absorption

The bulk absorption in resist material is described using the Beer-Lambert law [13], where the transmitted power or intensity into a film is related to absorption and thickness *by* $e^{-\alpha z}$. The impact of absorption on image transfer through a resist film will be a loss of a image contrast with increasing depth. Using this simple absorption model description for a

photoresist, there is a direct tradeoff between absorption and resist thickness. When the (*az)* product is set to 1.0, the resulting transmitted power through a film is 1/e. This 1/e depth for a given resist absorption is often used as a primary requirement for an imaging film. Figure 7 shows how resist absorption impacts images with TE and TM polarization. Plots are for image gradient values (*dI(x)/dx*) in a resist with an index of 1.5. Imaging conditions are as before and resist absorption is varied between 0.5 and 10 μm^{-1} (base-e). Images are focused in all cases at the top surface of the resist so that results can be compared. The imaging results are universal for any polarization. That is, there is a degradation in image gradient with increasing absorption and with increasing thickness. The loss from absorption can be offset with reduced thickness and visa versa. Polarization effects are important as the initial (non-absorbed) image is considered. Degradation in the TM image will be compounded with absorption effects, resulting in further loss of fidelity.

Defining first order absorption requirements is possible by comparing the absorption-induced depth limits to the optical focal depth limits. Using the Rayleigh paraxial DOF relationship (DOF ~ l/NA^2), a maximum usable optical image depth can be determined. For this example, a depth of 0.217 μm may be possible. Though this may be optimistic at oblique angles (and may be exaggerated by as much as 2X) [14], the use of off-axis illumination as a resolution enhancement technique could offset this loss because of the nature of the DOF improvement from oblique angles. For a resist to allow this full optical image depth, it should have an absorption no greater than 1/0.217 μm or 4.60 μm^{-1} to transmit power of 1/e to the bottom of the resist film. This corresponds to a base-10 absorption of ~2 μm^{-1}. Though 248nm and 193nm resist technologies provide sufficiently low absorption, the current 157nm resist situation may be problematic as absorption values below this level have not yet been demonstrated.

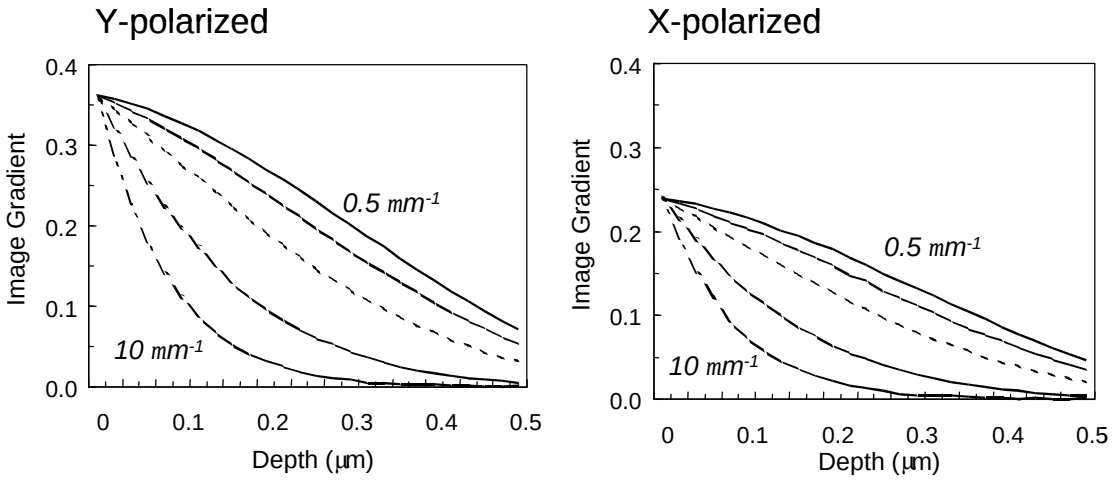

Figure 7. Image gradient plots showing the impact of resist absorption for Y (TE) polarized and X (TM) images.

2.2.4 Influence of resist diffusion

The diffusion of photoproduct can be described in terms of the convolution of the resist image with a spread function solution to Fick's Law. The spread function takes on a gaussian form $exp(-|Ar/L_d|^2)$, where L_d is the photoproduct diffusion mean free path (diffusion length), and *A* is a scaling factor. Figure 8 shows the impact of diffusion length values from 0 to 20 nm (where L_d is defined as $\sqrt{(2dt)}$, *d* is a diffusion constant and *t* is time) [7]. The gradient of the diffused resist image is plotted against image depth, focused at the top of the resist film as described above. As is the case for absorption, no polarization dependency exist for diffusion. Instead, loss in image contrast from the image spread resulting from diffusion will be compounded with any TM image polarization losses. Unlike absorption effects, diffusion losses can not be compensated for by resist thickness. This example shows how critical the photoproduct diffusion length becomes for low k_1 157nm lithography. There is a 2% loss in image gradient for every 1nm increase in diffusion length. It can be expected that diffusion length values approaching 10nm may be larger than tolerable, especially with a significant contribution of TM polarization.

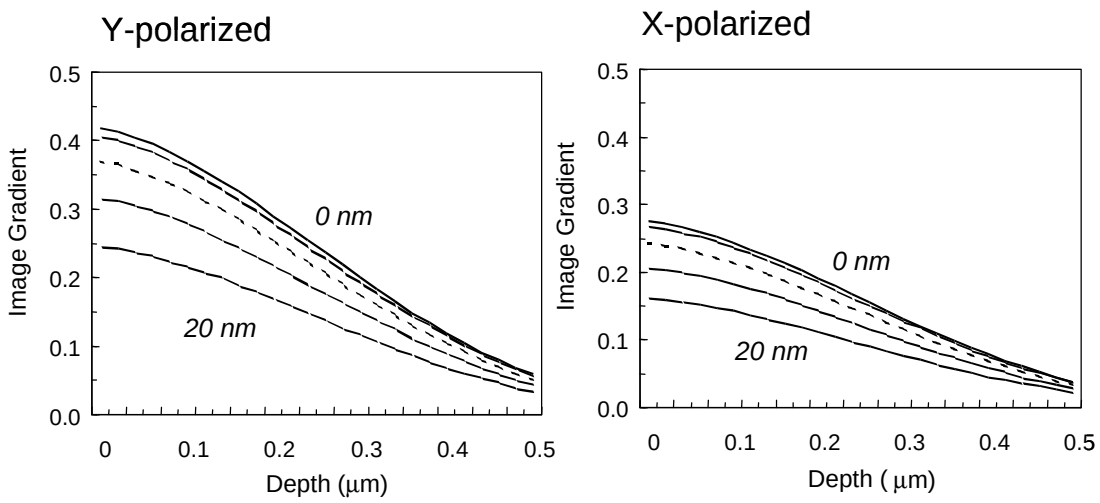

Figure 8. Image gradient plots showing the impact of diffusion for Y (TE) polarized and X (TM) images.

2.2.5 Induced spherical aberration

Considered as an optical component, a photoresist film is a "plane-parallel plate", with optical properties based on refractive index, absorption, and thickness. This is a well know effect and is shown in Figure 9. Imaging through a resist layer results in image displacement (a shift in focus position) but its impact is not limited to this effect. By applying aberration theory of two surfaces, imaging and aberration results can be evaluated. [9] The wavefront aberration function through the two surfaces of the plate can be written as:

$$W(\rho,\theta;h) = \alpha(\rho^4 - 4h\rho^3\cos(\theta) + 4h^2\rho^2\cos^2\theta + 2h^2\rho^2 - 4h^3\rho\cos\theta)$$

Where *h* is the separation of an object point from the optical axis, *a* is the weighted aberration coefficient, and ρ is the normalized radius of the pupil. The five terms of the function describe spherical, coma, astigmatism, defocus, and tilt respectively. For coherent or for symmetrical illumination, all terms of the wavefront aberration function drop out except for spherical. For a parallel plate, the aberration coefficient *a* is:

$$\alpha = \frac{t(n^2-1)}{8n^3S^4}$$

where *t* is the film thickness, *n* is refractive index and *S* is the distance of the focal position. The wavefront spherical aberration function becomes

$$W(\rho,\theta,0) = \frac{t(n^2-1)}{8n^3S^4}\rho^4$$

The impact of spherical aberration was addressed to some detail in previous sections. There is a polarization dependency to spherical aberration, resulting from the differences in interference between TE and TM image components. Figure 10 shows the effect. The derivative of the image gradient is plotted through focus for 1:1 dense line features varying from 60nm to 90 nm using 157nm wavelength and 0.85NA. The point where this derivative reaches zero indicates the best focus position for each individual line size. Spherical aberration is indicated by the disparity between best focus positions

between the features. Comparison of the TE and TM images show how spherical aberration effects can vary with polarization. The single plane spherical aberration induced by the resist film is larger for TE polarization. Additionally, there is a large offset in focus between polarization states. Figure 11 shows this, where best focus is plotted against line size for TE, TM, and unpolarized images. There is an offset between TE and TM polarization as well as a decrease in slope from TE to TM polarization. These effects will increase with refractive index and also as the range of imaging angles increases.

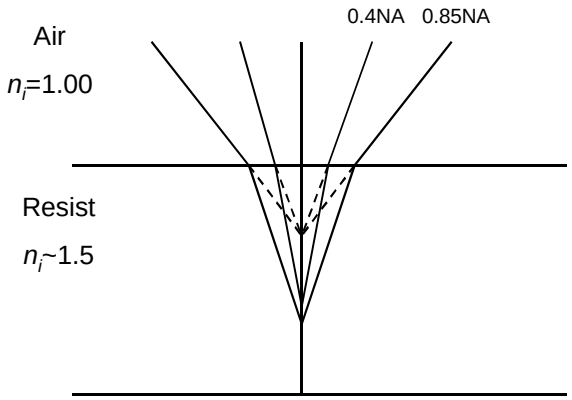

Figure 9. Spherical aberration induced by a resist film as a plane-parallel plate.

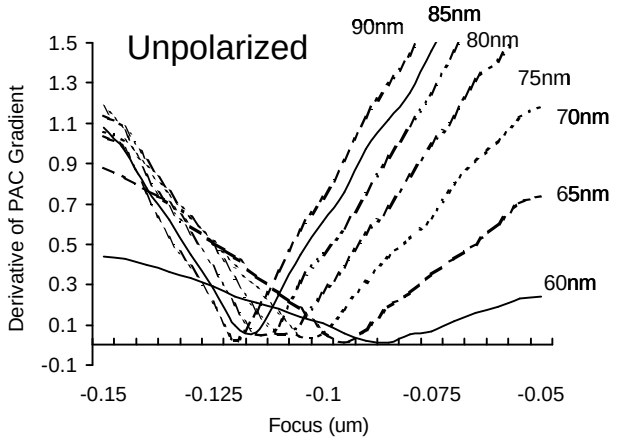

Figure 10. Spherical aberration plotted as the derivative of the image (PAC) gradient for unpolarized, X-polarized, and Y-polarized images.

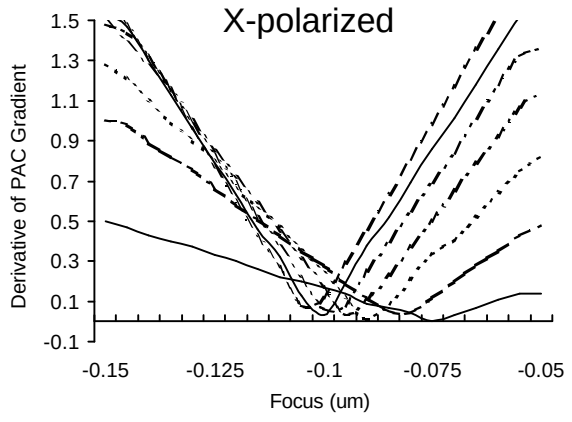

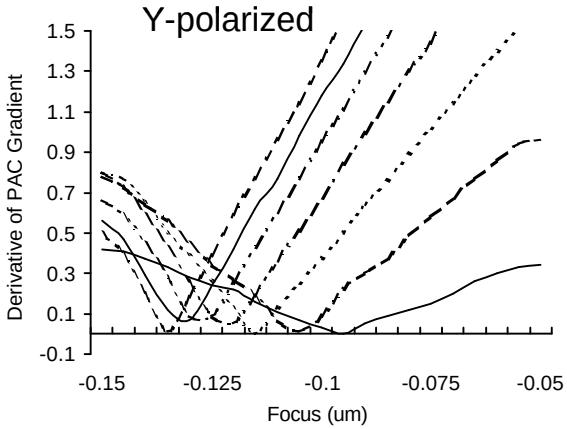

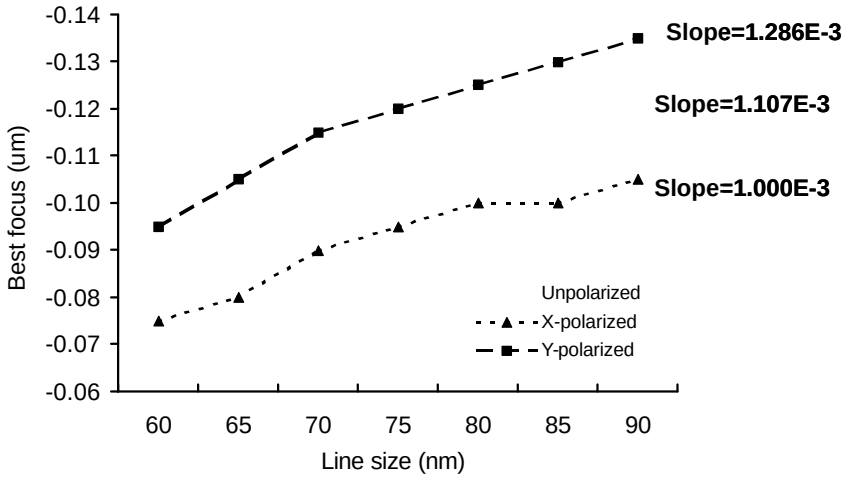

Figure 11. Spherical aberration plotted as best focus vs. line size for unpolarized, X polarized, and Y polarized images. Spherical aberration is indicated by the slope of the best focus plots.

3. POLARIZATION IMAGING

The analysis presented above verifies a preferential state of linear polarization (TE) that leads to a maximum image fidelity at high numerical apertures. Though it may seem advantageous to provide pure TE illumination to an imaging system, this presents problems as various mask feature orientations are considered. There is a general desire for global illumination that is either non-polarized or circularly polarized. However, opportunities at a local level may exist.

Localized polarization has been explored using the concepts of “wire grid polarizers”, consisting of periodic parallel features which can uniquely resolve orthogonal polarization components. Such grid arrays have been historically applied to various polarization applications. We have identified variations to the approaches that have been previously described. In one instance, grid arrays can be placed on the back side of a photomask. Through multiple patterning process steps, semi-localized grid “patches” can be placed over regions of device geometry with specific orientation, providing the desirable (TE) polarization illumination to photomask regions. A second application is a weak polarization effect that can be produced by proper orientation of OPC assist features to take advantage of a polarization induced edge enhancement that occurs at the boundaries of coarse pitch gratings (greater than $\lambda/2$ but near λ).

3.1 Wire-grid polarizers

Wire grids, generally in the form of an array of thin parallel conductors supported by a transparent substrate, have been used as polarizers for the visible, infrared and other portions of the electromagnetic spectrum. The key factor that determines the performance of a wire grid polarizer is the relationship between the center-to-center spacing, or period, of the parallel grid elements and the wavelength of the incident radiation. If the grid spacing or period is long compared to the wavelength, the grid functions as a diffraction grating, rather than as a polarizer, and diffracts both polarizations (not necessarily with equal efficiency) according to well-known principles. When the grid period is much shorter than the wavelength, the grid functions as a polarizer that reflects electromagnetic radiation polarized parallel to the grid elements, and transmits radiation of the orthogonal polarization.

The transition region, where the grid period is in the range of roughly one-half of the wavelength to twice the wavelength, is characterized by abrupt changes in the transmission and reflection characteristics of the grid. In particular, an abrupt increase in reflectivity, and corresponding decrease in transmission, for light polarized orthogonal to the grid elements will occur at one or more specific wavelengths at any given angle of incidence. These effects were first reported by Wood in 1902 [15] and are often referred to as "Wood's Anomalies". Subsequently, Rayleigh analyzed Wood's data and

had the insight that the anomalies occur at combinations of wavelength and angle where a higher diffraction order emerges.[16] Rayleigh developed the following equation to predict the location of the anomalies (which are also commonly referred to as "Rayleigh Resonances"):

$$l = p\,(n +/- \sin q)/m$$

where p is the grating period; n is the refractive index of the medium surrounding the grating; m is an integer corresponding to the order of the diffracted term that is emerging; and l and q are the wavelength and incidence angle (both measured in air) where the resonance occurs. For gratings formed on one side of a dielectric substrate, n in the above equation may be equal to either 1, or to the refractive index of the substrate material. The effect of the angular dependence is to shift the transmission region to larger wavelengths as the angle increases. This is important when the polarizer is intended for use as a polarizing beam splitter or polarizing turning mirror.

3.2 Back-side mask polarizers

Exploration of the feasibility of back-side mask polarizers for semi-local image enhancement has been carried out. Though several challenges become immediately evident (such as grating pitch requirement, patterning, tolerance to variation, metrology, handling, etc.), our recent results for longer wavelength lithography are encouraging and support additional work. Figure 12 shows the concept behind the back-side mask polarizer using an array of chromium metal lines. The general requirement for pitch (p) and height (h) of such structures are:

$$0.25 < h/p < 0.85$$
$$l/2 < p < l/(1.1n)$$

where n is the refractive index of the media surrounding the grid array. In the example of Figure 12, chrome lines 690Å high on a pitch of 275nm are used for a wavelength range between 430 and 500nm. Figure 13 shows the modeled results using EM field simulation for this wavelength range at incidence angle from 3° to 12°, corresponding to an NA of 0.85 in a 4X imaging system. The efficiency of polarization is quite high for these structures at ~65%.

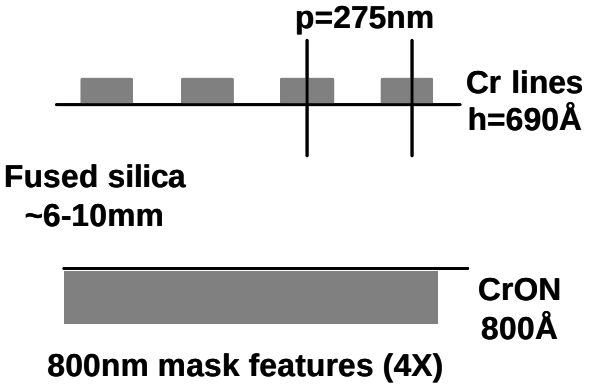

Figure 12. Schematic of back-side polarizers for 430-500nm wavelength application.

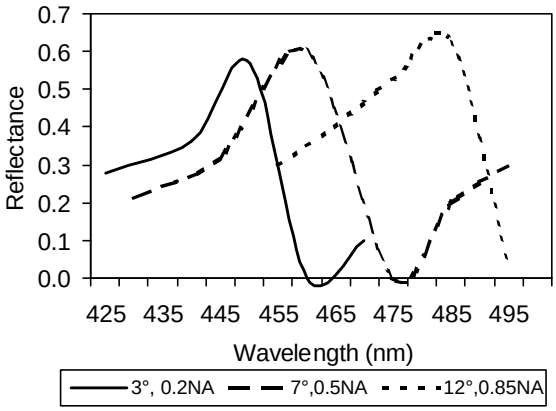

Figure 13. TE reflectance from chrome polarizer array.

3.3 Image-side "Zero-Order Gratings" (ZOGS)

Assist feature OPC has been utilized for several years to enhance the printability of semi-isolated geometry, especially in the presence of more dense features. In practice, multiple bars are often evenly spaced within a space opening between main features. The bar frequency does not coincide with that of the main features as it is generally beyond the diffraction limits of the imaging system. These bars can be considered zero-order gratings (ZOGs). No first order diffraction energy is collected from the bars making the bar frequency inconsequential. The result is that which would be expected if the space transmission was equivalently reduced.[7] It has been suggested that the effect of the adding multiple assist bars corresponds to the introduction of a frequency character to isolated features so as to resemble that of the dense features. This analysis is problematic on two accounts. First, the frequency of the bars is often beyond imaging limits, eliminating all but their zero diffraction order influence. Second, if the bars are placed at a frequency that matches that of the dense main features, the likelihood that the bars will print increases when using modified illumination. The frequency of the bars would be such that off-axis distribution of diffraction energy will increase the modulation and increase the depth of focus of the bars themselves. This is not a desirable effect. The implications go beyond this description since it also does not matter what orientation the bars take, either parallel or perpendicular to the main feature geometry. This added flexibility adds opportunity for design, especially when considering polarization effects.

Figure 14 shows a situation where two ZOG fields are in close proximity. If the grating pitch is sub-resolution, the features are not resolved. The transmission of each grating orientation is $(s/p)^2$ according to scalar calculation, where s is the space width and p is the pitch. Figure 15a shows the actual intensity field resulting from the combination of these two ZOG fields. An intensity edge exists at the interface between the horizontal and vertical fields, which results from the interaction of polarization fields induced by the gratings. The significance here is that the grating pitch may be sub-resolution but not necessarily sub-half-wavelength. For example, with a 193nm imaging system operating at 0.70NA and 4X, a pitch value of 250 nm on the mask is sub-resolution. The bar size corresponds to assist feature width, on the order of 30 to 50 nm. Though the effect is weak, as seen in the intensity plot of Figure 15b for incoherent illumination, this effect could be utilized to enhance the effect of assist bar OPC. Figure 16 depicts a 90 nm main line features placed between horizontal and vertical ZOG arrays of 30nm (bar size). Figure 17 shows how the aerial image in the region of perpendicular bars is superior to the image in the region of parallel bars. The weak polarization induced edge enhancement increases image log slope (ILS) by as much as 30% for unpolarized illumination.

4. CONCLUSIONS

We have shown that extreme-NA imaging requires that polarization effects be taken into consideration. As numerical apertures above 0.70 are pursued, the most oblique angles corresponding to outermost portions of the lens pupil will be used, such as with strong off-axis illumination or with phase shift masking. In these cases, the differences in TE and TM image modes are significant. As images are directed into a photoresist film, the resist refractive index, absorption, diffusion, and induced aberration will impact image fidelity. The design of the optical properties of photoresist films for extreme-NA application should take this into account. General requirements may be:

- Higher refractive index resist materials for unpolarized imaging
- Lower refractive index resist materials for TE polarized imaging
- Optical absorbance less than 1/DOF
- Thickness less than the 1/e absorption depth
- Diffusion length less than 10nm for minimal image loss
- High resist contrast (as well as thin resist for maximum contrast)
- Strong top anti-reflective layers coated for large (oblique) angle reflectivity control

The advantages of using a single polarization mode (TE) can be utilized through local and semi-local polarization methods at the mask. We have introduced two such concepts as wire-grid polarizer structures.

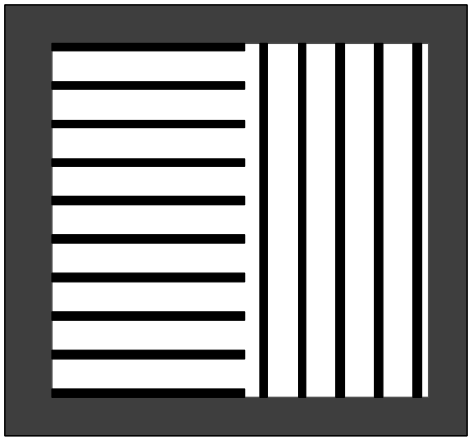

Figure 14. Opposing ZOG fields.

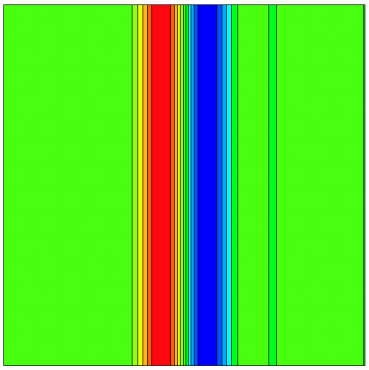

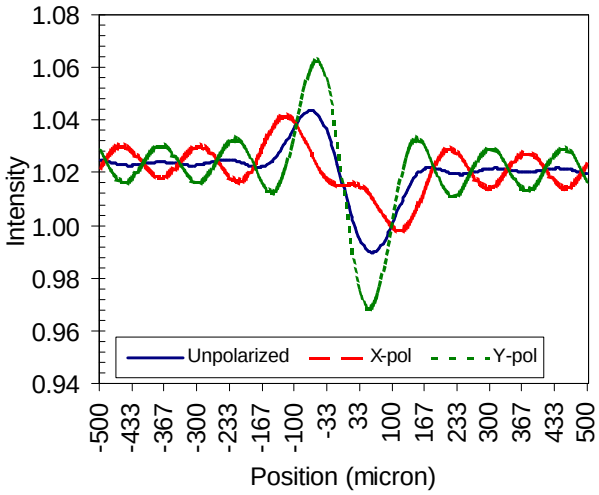

Figure 15a and b. Intensity image for ZOG fields.

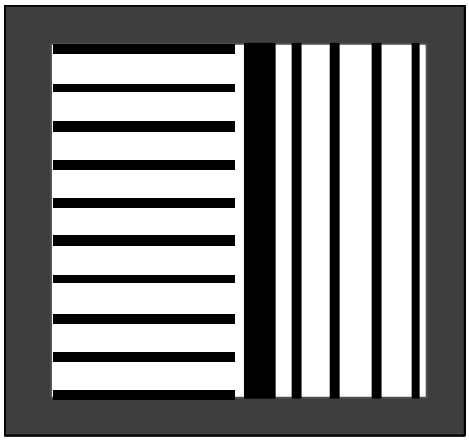

Figure 16. 90 nm line between horizontal and vertical 30nm ZOG fields.

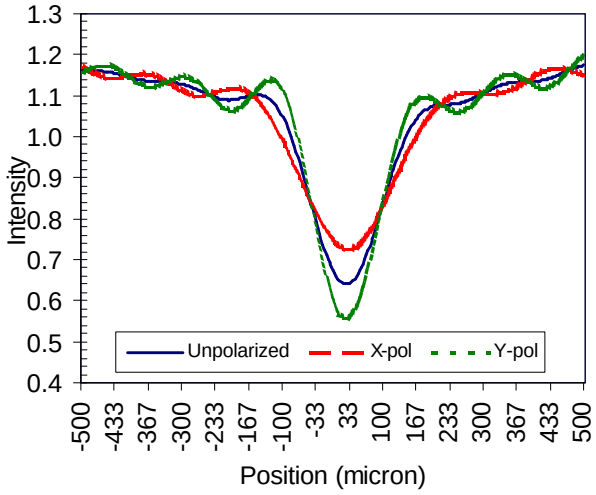

Figure 17. Aerial image of 90 nm line in ZOG fields using 193nm wavelength, 0.95NA, and 4X reduction.

5. REFERENCES

[1] D.G. Flagello, A.E. Rosenbluth,, "Lithographic tolerances based on vector diffraction theory," *J. Vac. Sci. Technol. B*, **10(6),** pp 2997-3003, 1991.

[2] M. Born and E. Wolf, *Principles of Optics*, 6th edition, pp. 113-117, Pergamon Press, Oxford, 1980.

[3] D.G. Flagello, A.E. Rosenbluth, C. Progler, J. Armitage, "Understanding high numerical aperture optical lithography," *Microelectronic Engineering*, **17**, pp. 105-108, 1992.

[4] D.A. Bernard and H.P Urbach, "Thin-film interference effects in photolithography," *J. Opt. Soc. Am. A*, **8**, 1, pp. 123-133, 1991.

[5] C. Mack, *Inside Prolith*, pp. 31-35, FINLE Technologies, Austin, Texas, 1997.

[6] http://public.itrs.net/Files/2001ITRS/Litho.pdf.

[7] B.W. Smith, "Mutual Optimization of resolution Enhancement Techniques", *J. of Microlithography, Microfabrication, and Microsystems*, 2, 2002.

[8] Images produced using Prolith v. 7.0 Vector model, FINLE technologies, 2001.

[9] H.J. Levinson and W.H. Arnold, "Focus: the critical parameter for submicron lithography", *J. Vac. Sci. Tech*., **B5**, pp. 293-298, 1987.

[10] V. Mahajan, *Aberration Theory made Simple*, pp. 30-34, SPIE Press, Bellingham, WA, 1991.

[11] J.C. Dainty and R. Shaw, *Image Science*, pp. 204-209, Academic Press, San Diego, CA, 1974.

[12] M. Born and E. Wolf, pp. 41-47.

[13] F. Grum and R.J. Becherer, Optical Radiation Measurements Vol. 1, pp. 279-280, Academic Press, San Diego, CA, 1979.

[14] B.J. Lin, "The k_3 coefficient in nonparaxial l/NA scaling equations for resolution, depth of focus, and immersion lithography," *J. of Microlithography, Microfabrication, and Microsystems*, 1, pp. 7-12, 2002.

[15] R. Wood, *Philosophical Magazine*, September 1902.

[16] Lord Rayleigh, *Philosophical Magazine*, vol. 14(79), pp. 60-65, July 1907.